Titre: Title:	Effects of weathering on the properties and fate of secondary microplastics from a polystyrene single-use cup
Auteurs: Authors:	Olubukola S. Alimi, Dominique Claveau-Mallet, Mathieu Lapointe, Thinh Biu, Lan Liu, Laura M. Hernandez, Stéphane Bayen, & Nathalie Tufenkji
Date:	2023
Type:	Article de revue / Article
Référence: Citation:	Alimi, O. S., Claveau-Mallet, D., Lapointe, M., Biu, T., Liu, L., Hernandez, L. M., Bayen, S., & Tufenkji, N. (2023). Effects of weathering on the properties and fate of secondary microplastics from a polystyrene single-use cup. Journal of Hazardous Materials, 459, 131855 (11 pages). https://doi.org/10.1016/j.jhazmat.2023.131855

Effects of Weathering on the Properties and Fate of Secondary Microplastics from a Polystyrene Single-Use Cup

Journal of Hazardous Materials

Olubukola S. Alimi[a,d], Dominique Claveau-Mallet[a,b], Mathieu Lapointe[a], Thinh Biu[a], Lan Liu[c], Laura M. Hernandez[a], Stéphane Bayen[c, *] and Nathalie Tufenkji[a, *]

[a]Department of Chemical Engineering, McGill University, Montreal, Quebec H3A 0C5, Canada
[b]Department of Civil, Geological and Mining Engineering, Polytechnique Montreal, 2900 Edouard-Montpetit, Montreal
[c]Department of Food Science and Agricultural Chemistry, McGill University, Montreal, 21111 Lakeshore, Ste Anne de Bellevue
[d]Department of Civil and Environmental Engineering, University of Alberta, Edmonton, T6G 1H9, Canada

* Co-corresponding author: oalimi@ualberta.ca

Graphical Abstract

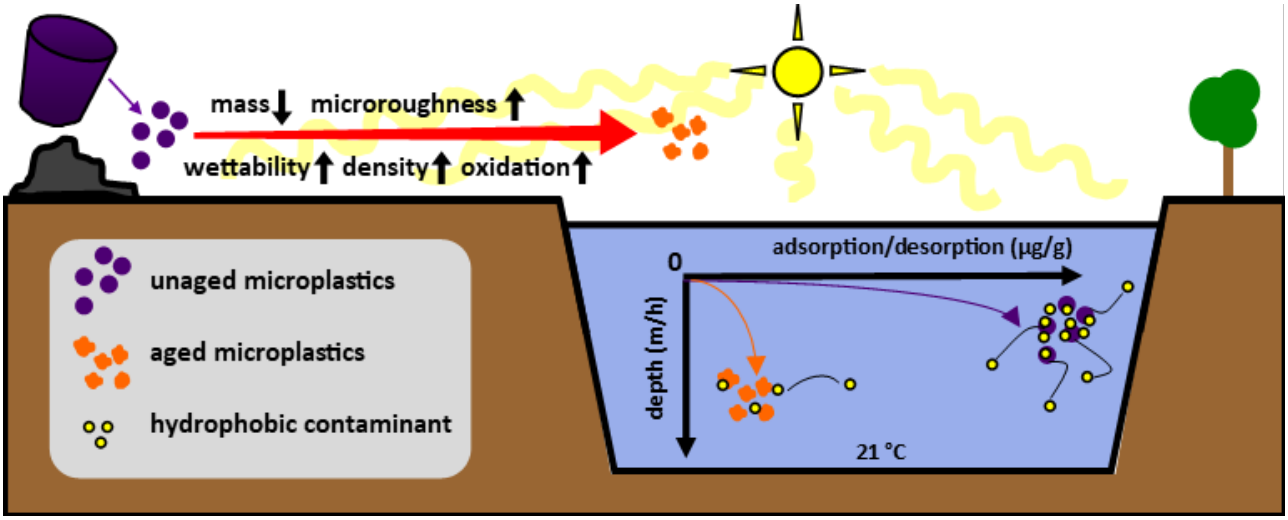

Abstract

In this work, we probed the changes to some physicochemical properties of polystyrene microplastics generated from a disposable cup as a result of UV-weathering, using a range of spectroscopy, microscopy, and profilometry techniques. Thereafter, we aimed to understand how these physicochemical changes affect the microplastic transport potential and contaminant sorption ability in model freshwaters. Exposure to UV led to measured changes in microplastic hydrophobicity (20 to 23% decrease), density (3% increase), carbonyl index (up to 746% increase), and microscale roughness (24 to 86% increase). The settling velocity of the microplastics increased by 53% after weathering which suggests that UV aging can increase microplastic deposition to sediments. This impact of aging was greater than the effect of the water temperature. Weathered microplastics exhibited reduced sorption capacity (up to 52% decrease) to a model hydrophobic contaminant (triclosan) compared to unaged ones. The adsorption of triclosan to both microplastics was slightly reversible with notable desorption hysteresis. These combined effects of weathering could potentially increase the transport potential while decreasing the contaminant transport abilities of microplastics. This work provides new insights on the sorption capacity and mobility of a secondary microplastic, advances our knowledge about their risks in aquatic environments, and the need to use environmentally relevant microplastics.

Keywords. vertical transport, plastic pollution, organic pollutant, plastic degradation, contaminant mobility, food and beverage container

1. Introduction

There is growing concern about the environmental risks posed by microplastic pollution to ecosystems. Microplastics (< 5 mm) are often classified as either having primary (intentionally produced pellets/beads) or secondary origin (tiny fragments from single-use or other plastic debris). Secondary microplastics are thought to be found in larger quantities (nearly two-thirds of all microplastics) in the ocean compared to primary ones (Boucher and Friot, 2017). A bibliometric analysis revealed that majority (~90%) of studies aimed at understanding the risks associated with microplastic pollution have been carried out with unaged microplastics (Alimi et al., 2022). The few effect studies that attempt to use environmentally relevant microplastics (aged microplastics) focused on weathering plastics from primary sources rather than those originating from plastic debris (secondary source). An estimate shows that 46% of global plastic debris originates from single-use plastic packaging material (Geyer, 2020), which can become film fragments in the environment. Numerous field studies also detect microplastic films in the environment and biota, hence there is a need to understand the behavior of microplastic films (i.e. flat microplastics) when investigating risk. Although there are several governmental and institutional legislations and movements to reduce the global plastic footprint (especially concerning single-use plastics), these measures are still in their infancy. Hence, the burden of plastic pollution will continue in the foreseeable future. Studies predict that plastic emissions and exposure to the environment will increase even with the current rate of intervention strategies (Borrelle et al., 2020; Lau et al., 2020).

Throughout the lifecycle of microplastics, they experience multiple forms of weathering such as photodegradation, thermal degradation, biofouling, either simultaneously or sequentially (Alimi et al., 2020; Andrady, 2011; Jahnke et al., 2017). These processes will impact microplastics' properties and buoyancy, and hence their settling behavior which will either lead to long-range transport or accumulation near the source of release in aquatic environments. Understanding the sinking behavior of microplastics is particularly important in designing remediation strategies (Van Melkebeke et al., 2020), predicting the concentration of microplastics in the water column, identifying pollution hotspots within the water column (Lobelle et al., 2021) or microplastic release and resuspension in lakes (Zhang et al., 2020). However, in the current literature, there is a lack of understanding about the effect of weathering on the sinking behavior and residence time of

microplastics, especially microplastic films/sheets. Although the effect of biofouling on the vertical transport of microplastics has been theoretically modeled (Kooi et al., 2017), only a few experimental studies have attempted to investigate the impact of weathering on the settling behavior of microplastics, with contrasting findings. Waldschlager et al. showed that microplastics collected from a fluvial environment settled slower compared to unaged microplastic samples (Waldschläger et al., 2020; Waldschläger and Schüttrumpf, 2019). Nguyen et al. also reported that microbe-associated polyurethane microplastics have sinking rates two times slower than unaged ones (Nguyen et al., 2020). In contrast, two studies showed that biofouled microplastics exhibit higher settling velocities than unaged ones (Kaiser et al., 2017; Miao et al., 2021). Clearly, there is a need to better understand the crucial role of weathering processes in altering the physicochemical properties and behavior of microplastics.

Microplastics have been shown to act as sources and sinks for other emerging contaminants in the environment (Rochman et al., 2013). However, there exists contradictory reports on whether microplastics can significantly facilitate the mobility of emerging contaminants. Triclosan is an example of a hydrophobic contaminant with increasing concern about its fate. It is an anti-microbial additive used in some personal care products, known to be toxic and widely detected in the aquatic environment (Pullaguri et al., 2023). A substantial number of studies have investigated the sorption/desorption capacity of unaged primary microplastics, yet, our understanding of the interaction of other contaminants with microplastics from secondary sources (e.g. single-use plastics) is still limited.

Therefore, to address some of these gaps, the objective of this work is to systematically investigate how UV weathering alters the properties of secondary microplastics (4.5 mm) sourced from a single-use disposable product, and how these changes subsequently affect particle fate and behavior in a simulated freshwater system. For this purpose, microscopy, spectroscopy, and profilometry techniques were used to characterize the surface and bulk properties of the microplastics before and after exposure to UV irradiation. The adsorption and desorption of the model hydrophobic contaminant, triclosan to the aged and unaged microplastics were also measured. Experimentally determined settling velocities were coupled with a model to simulate the vertical transport and contaminant-facilitated transport potential of microplastics in freshwater

systems. Model simulations on the effects of weathering on the transport of microplastics of different shapes are presented for 220 μm sized microplastics.

2. Materials and methods

2.1 Plastic source and UV weathering treatment

Single-use plastic cups (Cogan, #13-3001859) were purchased from a Dollarama store in Montreal, Canada in 2019. A heavy-duty revolving leather punch (SE 7924LP) was used to generate circular microplastic disks with 4.5 mm diameter from the disposable cups. Afterwards, the microplastics were rinsed thoroughly with reverse osmosis water (Biolab Scientific). Two treatments of these microplastics were used for all subsequent experiments. Some samples were kept at room temperature in the dark (to minimize light exposure) before use and were labelled unaged microplastics. A separate batch of samples was placed in a glass plate containing 10 mM NaCl solution at pH ~6 (to mimic freshwater) (Katz et al., 1997) and exposed to UV irradiation in a weathering chamber for 8 months (called aged microplastics). The weathering chamber was kept at a temperature of 27 °C. The UV light consisted of both UVA and UVB bulbs (306 nm; Topbulb G15T8E, 350 nm; Topbulb, Eiko F15T8/BL and 365 nm; Hikari Lamps) with total intensity of ~35 W/m^2. During weathering, the microplastics were gently stirred at 35 rpm which ensured exposure of both sides of the microplastics to the UV radiation. After weathering, the microplastics were thoroughly rinsed with reverse osmosis water, air-dried, and stored in the dark at room temperature in a desiccator for further use.

2.2 Characterization of microplastics

The change in microplastic mass after weathering was quantified using an ultra-micro analytical balance (S4, Sartorius) having a weighing accuracy/sensitivity of 0.0001 mg. The density of the unaged and aged microplastic was quantified using the titration method described in ISO 1183-1 (ISO-1183-1, 2019). Briefly, the microplastics were placed in a glass beaker with 50 mL reverse osmosis water. Then, small droplets of concentrated zinc chloride (#MKCG2036, Sigma Aldrich) solution were added to the beaker while the liquid was stirred. This process was repeated until the microplastic floated to the surface of the liquid. To determine the density, 1 mL of the final solution was then weighed on an analytical balance (MS104TS/00, Mettler Toledo). The thickness of each

109 microplastic was measured using a digital caliper (Mastercraft, Digimatic) with 0.02 mm accuracy.
110 The crystallinity of the microplastic was determined using the density measurement method by
111 estimating the weight fraction crystallinity of the microplastic (equation S1) as described in section
112 S1.

113 The surface functional groups of the unaged and aged microplastics were characterized using a
114 Fourier-transform infrared spectrometer (FT-IR, Spectrum II, PerkinElmer) in attenuated total
115 reflectance (ATR) mode with a single bounce diamond. Microplastic disks were analyzed in the
116 region 400-4000 cm^{-1} with 32 scans at 4 cm^{-1} resolution. The specified-area-under-band method
117 (Almond et al., 2020) was adopted to calculate the ratio of the integrated band under the carbonyl
118 region (1650–1800 cm^{-1}) and a reference absorption peak band (C-H) (Saron et al., 2007) (640–
119 720 cm^{-1} centered at 696 cm^{-1}). Spectragryph software (v1.2.15) was used for peak analysis and
120 normalization. X-ray photoelectron spectroscopy (XPS) with etching was used to analyze the
121 oxidation profile of the aged and unaged microplastics. Briefly, the spot size was set to 200 µm,
122 the etching parameters set to 500 eV with a low current (etching rate of 0.21 nm/s in Ta_2O_5), and
123 three levels of etching were measured (0 s, 3 s, and 6 s). Spectra of the C1 and O1 peaks were
124 collected.

125 The surface hydrophobicity of the microplastics was measured using the sessile water contact
126 angle method on an OCA 20 Goniometer (DataPhysics Instruments). The instrument is equipped
127 with an automated microliter syringe and a digital camera. For both aged and unaged microplastics,
128 a total of 12 disks (6 each for the inner and outer surface of the original cup) were used. Briefly, 3
129 µL of water was dispensed on each sample surface and measurement was carried out within 3 s.
130 Measurement on each sample was repeated twenty times on different areas of the plastic surface.

131 The surface morphology of the microplastics was characterized using scanning electron
132 microscopy (FEI Inspect F50) with accelerating voltage of 5 kV. Samples were thoroughly rinsed
133 with reverse osmosis water and dried; thereafter, sample surfaces showing the inner and outer parts
134 of the cup were coated with a 3 nm layer of platinum before measurement (Leica Microsystems
135 EM ACE600 Sputter Coater). An optical profilometry technique was used to quantitatively
136 characterize the surface roughness of the plastics (Zygo NexView 3D) with Mx software. The
137 Coherence Scanning Interferometry (CSI) mode with high z-resolution, signal oversampling and
138 20 µm scanning length were adopted. All data were analyzed and extracted from the Mx software

to obtain the profile parameters. Briefly, at least 12 microplastics (6 each for the inner and outer surface of the original cup) for each weathering condition were mounted on a glass slide with a double-sided tape before each measurement. The Brunauer–Emmett–Teller (BET) specific surface area was measured using the nitrogen adsorption method (Tristar II Plus, Micromeritics). Prior to the analysis, microplastic samples (minimum of 40 pieces) were degassed to remove any contaminants at 120 °C in vacuum overnight.

The tensile strength of the microplastic was estimated with a Shimadzu EZ Universal Tensile tester. For tensile strength measurements, ASTM D638 (Standard Test Method for Tensile Properties of Plastics) and D882 (Standard Test Method for Tensile Properties of Thin Plastic Sheeting) were used with slight modifications to the sample size. Rectangular plastic strips (70×10 mm) from the disposable cups were used for all measurements and these strips underwent the same weathering procedure as the 4.5 mm disks.

2.3 Settling experiment

The settling velocity of the microplastics was measured using a cylindrical column (50 cm height and 10 cm diameter) following the procedures described in previous studies (Van Melkebeke et al., 2020; Waldschläger and Schüttrumpf, 2019). Microplastics were placed at the center of the column, approximately 1 cm below the water surface using stainless-steel tweezers, and released to fall freely. The time each particle took to travel to a depth of 29 cm was recorded with a stopwatch. This 29 cm depth is between two upper and lower excluded sections (10 cm each) of the water column and was selected because the particles achieved terminal velocity at a depth of ~10 cm). Following procedures described elsewhere (Waldschläger and Schüttrumpf, 2019), the mid-section (29 cm) was divided into two parts, and the similar microplastic velocities in both sections confirmed there was no further acceleration after 10 cm. The fluid in the settling column contained 10 mM NaCl at pH 6 to mimic freshwater. Microplastics were pre-wetted by immersing in the same fluid at least 2 days before each experiment. The temperature of the fluid for all experiments was kept at 20 °C or 1 °C. All experiments at 1 °C were carried out in a cold chamber (Danby, DWC032A2BDB) to maintain the temperature during the experiments. To validate the measured settling velocities, the settling velocity of standard polystyrene spheres of a comparable size as the microplastics used in this study was investigated. The polystyrene spheres (Cospheric LLC, Lot # 30199318-07) had a mean diameter of 4.7 ± 0.05 mm and a density of 1.05 kg/m^3. The

theoretical Stokes settling velocity of the model spheres (calculated as 7.4 cm/s) was compared with the measured settling velocity (7.0 ± 0.1 cm/s). Since the average measured settling velocity deviated by only 5% from the theoretical value, the protocol used for measuring the microplastic settling velocity was deemed valid and reliable.

2.4 Adsorption kinetics and isotherm experiment

Triclosan (Sigma-Aldrich) was used as the model hydrophobic contaminant (log K_{ow} = 4.76) in this study as it is often detected in freshwater and treated wastewater (Barrett et al., 2022; Lindström et al., 2002). Batch kinetic adsorption experiments were conducted at concentrations of 20 and 100 µg/L triclosan, respectively. Isotherm experiments included two additional concentrations of ~50 and ~150 µg/L triclosan. These concentrations were chosen to be above the limit of detection of the LC-MS instrument used but close to same order of magnitude of some reported concentrations. Some studies report up to 5.37 µg/L in treated wastewater effluent (Kumar et al., 2010) and 5.16 µg/L in surface water (Ramaswamy et al., 2011). Preliminary experiments showed that the time needed to reach equilibrium was approximately 21 days, hence all experiments were conducted for at least 21 days. For each condition, 7 disks of either unaged or aged plastic (~30 mg total) were added to 40 mL triclosan solution in amber glass vials (Sigma-Aldrich) and shaken in an end-to-end rotator (Boekel Scientific) at 60 rpm. All triclosan solutions were prepared in background electrolyte of 10 mM NaCl. At each sampling time point, each aliquot was spiked with 50 µg/L of internal standard (triclosan-d_3 from CDN Isotopes), filtered through a 0.22 µm membrane filter (PTFE syringe filter, Canadian Life Science) and stored in a freezer (-4°C) before analysis. Control samples with triclosan in background electrolyte solution without microplastics were also shaken in the rotator during all experiments to monitor contaminant loss. All experiments were performed at room temperature (~20-22 °C). Solution pH was at 6.0 ± 0.2 throughout all experiments.

2.5 Desorption experiment

Triclosan desorption kinetics and isotherm were measured immediately after each respective adsorption phase. Briefly, the microplastic disks were transferred from each adsorption vial using tweezers into 40 mL triclosan-free 10 mM NaCl solution in amber vials. The liquid phase triclosan concentration in each aliquot was monitored for 21 days to ensure that equilibrium was reached.

At each sampling time point, each vial was spiked with 50 µg/L of internal standard (triclosan-d_3), filtered through a 0.22 µm membrane filter (PTFE syringe filter, Canadian Life Science) and stored in a freezer (-4 °C) before analysis.

2.6 Analytical instrumentation

The triclosan concentration in all adsorption experiments was measured by an Agilent 1290 Infinity II LC system coupled to a 6545 Q-TOF-MS (Agilent Technologies, Santa Clara, USA). The LC separation was done with a Poreshell120 EC-C18 analytical column (3 mm×100 mm, 2.7 µm; Agilent Technologies) connected with a Poreshell120 EC-C18 guard column (3 mm×5 mm, 2.7 µm; Agilent Technologies;). The mobile phase A was HPLC water and the mobile phase B was acetonitrile/methanol mixture (50:50 v/v). Ammonium acetate (5 mM) was added to both mobile phases A and B to improve the electrospray ionization (ESI) efficiency. Samples were kept at 4 °C in the multisampler compartment. Details of HPLC and MS parameters are presented in Table S1. During the sample run, reference ions (112.9856 and 1033.9881 *m/z* for ESI in negative mode) were used for automatic mass recalibration of each acquired spectrum.

2.7 Transport distance simulation

Here, we aimed to simulate the effect of aging on microplastic transport and contaminant co-transport potential. To predict the transport of smaller microplastic disks (≤ 220 µm), an equation for the theoretical settling velocity was developed based on Newton's law (balance of forces acting on a single particle falling in a fluid) by assuming the shape of a disk (detailed derivation is provided in equations S2-S4, supplementary information, section S2). This equation is given as;

$$V_p = \sqrt{\frac{2gh\,(\rho_p - \rho_l)}{C_D \rho_l}} \tag{1}$$

where V_p = terminal settling velocity, C_D is the drag coefficient which is a function of the Reynolds number (R_e), ρ_l = density of the fluid, ρ_p = density of the particle, h = thickness of the microplastic disk.

When $R_e < 1$, equation 2 was obtained while C_D was calculated using the Stokes equations (see eq S3 in SI). A correction factor (C_f) was applied to the C_D of the aged microplastics to account for

any effects of aging on the material surface properties (e.g., diameter, wettability, roughness). This correction factor allows the simulation of the effect of aging on the settling velocities and travel distance of microplastics. Equation 2 was used for simulations presented in section 3.2.

$$V_p = \frac{2ghd_e(\rho_p - \rho_l)}{20.4C_f\eta} \quad (2)$$

where η = dynamic viscosity, d_e is the disk equivalent diameter.

2.8 Data and statistical analysis

All adsorption experimental data were fitted using the linear, Langmuir and Freundlich isotherms. The kinetics were modeled using the pseudo-first and second-order kinetic models. The Solver Add-in Excel tool was used for all curve fitting. All adsorption equations used are summarized in Table S1 and the non-linear forms of these models were used in fitting all experimental data for comparison. Where necessary, statistical significance was evaluated using one-way ANOVA and Tukey HSD mean comparison. All statistical analysis was performed using OriginPro software (version 9.8.0.200).

3. Results and discussion

3.1 Changes to physical and chemical properties of microplastics after weathering

After aging, we observed that the microplastic disk color changed from white translucent to yellow opaque (Figure 1a, b). The yellowing of polystyrene is often observed as a result of the free radicals generated by the chromophore during photooxidation (Andrady et al., 1998). It is important to note that the bulk plastic cup had a glossy outer layer which was still preserved after aging for all disk samples (Figure S1). SEM images showed slight changes on the surface of the aged microplastics (Figure S2). From observation, the outer side of the aged cup seemed to show higher pitting in comparison to the unaged surface, however, this was not comprehensively quantified. The inner side of the cup appeared more irregular than the outer side, however, when comparing the aged sample with the unaged there were no obvious changes (Figure S2). To quantitatively characterize and compare the surface roughness of the unaged and aged disks, an optical profiler was used. The

results of surface topography characterization are shown in Figure 1e, f (2D profile), Figure S3 (3D isometric view), and Figure 1i, j (roughness parameters of interest, S_a the average surface roughness, and S_z the peak to valley height). By inspecting the 2D and 3D scans, we observed deeper valleys and higher peaks (blue and red regions, respectively) on the surface of the aged microplastics compared to the unaged ones. For both cases, the outer side of the cup was considerably smoother. This was confirmed in the measured S_a and S_z parameters on 167×167 μm^2 areas (Figure 1i, j). For all conditions, S_a and S_z were lower for the outer side compared to the inner side. After aging, we observed a slight increase in S_a (for the inside surface) and a larger increase in S_z (both $p < 0.05$). This shows that weathering increased the microscale roughness of the microplastics which complements the increase in Brunauer–Emmett–Teller specific surface area measured (0.34 and 0.95 cm^2/g for unaged and aged plastics, respectively).

The measured wettability of the microplastics showed that the outer surface of the unaged microplastics had the highest contact angle (Figure S4). After weathering, the contact angle of the microplastics decreased, indicating an increase in hydrophilicity of the material, as seen in Figure 1g, h. When comparing the outer and inner surfaces of the microplastics, we observed that the outer surface was more hydrophobic (99 ± 5 and 80 ± 5 vs 91 ± 5 and 70 ± 4° for both unaged and aged microplastics, respectively, $p<0.05$). This translates to a decrease in the contact angle of 23% for the inner surface and 20% for the outer surface after weathering. Leaching of additives from the plastic material may also have contributed to the increased hydrophilicity of the material. Similar trends of decreased water contact angle of aged polystyrene microplastics compared to unaged plastics were recently reported (Krause et al., 2020; Van Melkebeke et al., 2020).

The mass changes after weathering (Figure 1k) showed a slight decrease (14%) in the average mass after weathering, however, this change was not statistically significant ($p>0.05$). The average diameter also did not significantly change after weathering (0.45 to 0.44 ± 0.03 mm). This shows how long it may take plastic debris to completely break down in the environment. Interestingly, we observed an increase in the density of the aged microplastics, by 3% (from 1.04 ± 0.004 to 1.07 ± 0.004 g/cm^3, $p<0.05$). In polymers, density changes are typically associated with either changes in crystallinity, changes in mass or volume (diameter and thickness) or loss of plasticizers, biofouling. UV irradiation has been shown to increase crystallinity due to the close and regular packing of the polymer chains (Rowenczyk et al., 2020). Compared to amorphous areas, the

crystalline part of a polymer is more densely packed (Rudin and Choi, 2013), hence, an increase in crystallinity could lead to increased density (decreased specific volume). It was previously observed that UV exposure led to an increase in nylon density (Stowe et al., 1973). From the weight fraction crystallinity calculated for unaged and aged microplastics (equation S1), the crystallinity of the microplastics increases from 0 to 37%. Therefore, the increase in density can be attributed to an increase in crystallinity of the microplastics.

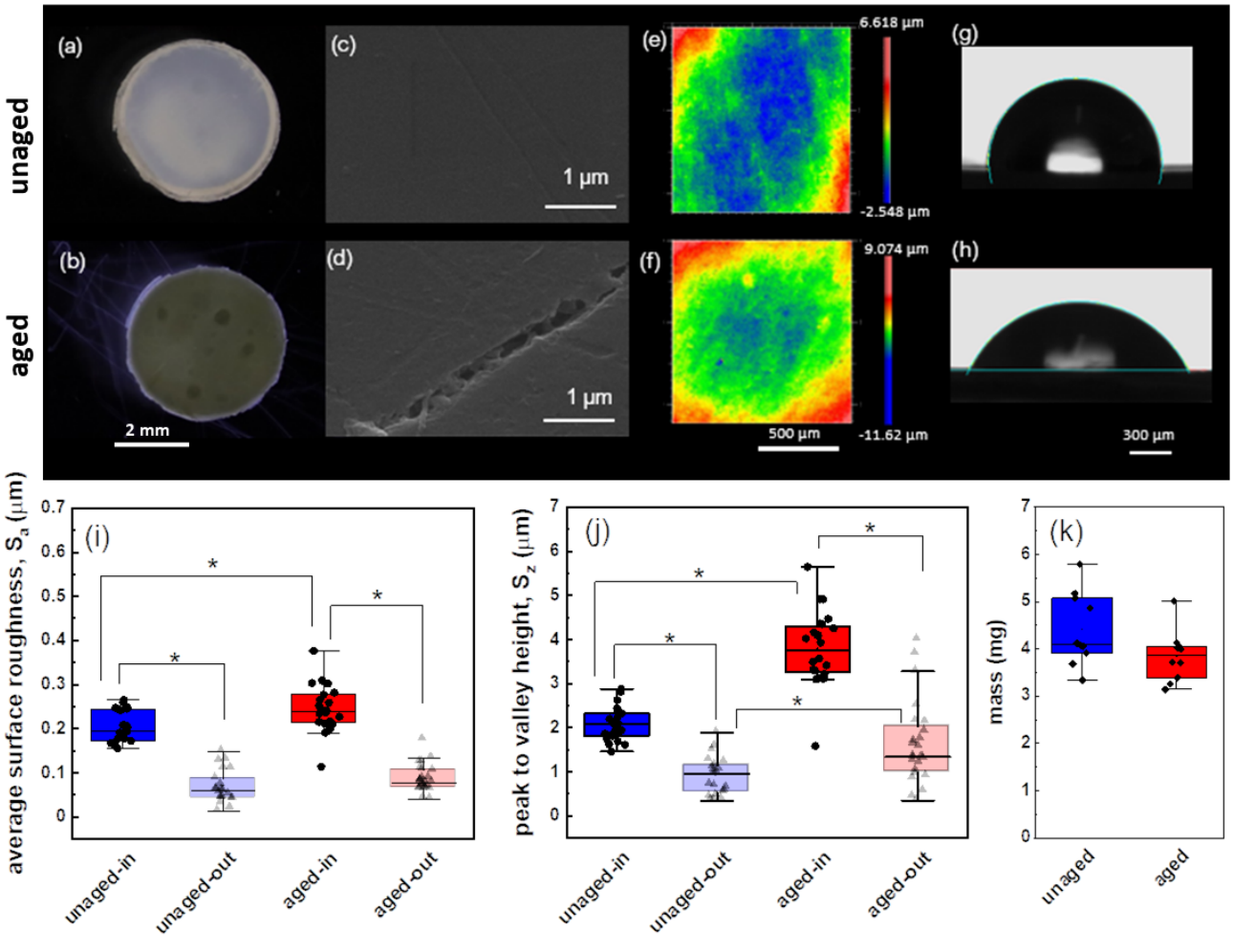

Figure 1. Physical characterization of the unaged and aged microplastics. (a, b) colour changes of the microplastic, (c, d) surface morphology of microplastics (outer side) using SEM, (e, f): roughness profile of the microplastics (inner side) using a profilometer, (g, h) representative image of water droplet for contact angle measurement on unaged and aged microplastics (inner side), (i, j) roughness parameters, S_a and S_z at 50× magnification, (k) mass change of microplastic disks before and after weathering. Unaged-in and aged-in refer to the inner surface of the original cup, while unaged-out and aged-out refer to the outer surface of the cup.

Table 1. Summary of parameters related to changes in physical, chemical, and mechanical properties of the microplastics after aging

Property	unaged-in	unaged-out	aged-in	aged-out
Contact angle (°)	91 ± 5	99 ± 5	70 ± 4	80 ± 5
Carbonyl index (-)	0.024 ± 0.012	0.0031 ± 0.0051	0.068 ± 0.042	0.026 ± 0.011
	unaged		**aged**	
Young's modulus (MPa)	496 ± 54		597 ± 178	
Ultimate elongation (-)	0.074 ± 0.0076		0.023 ± 0.0019	
Thickness (mm)	0.25 ± 0.048		0.24 ± 0.045	
BET specific surface area (cm^2/g)	0.34		0.96	
Density (g/cm^3)	1.04 ± 0.004		1.07 ± 0.005	

The unaged microplastics were confirmed as polystyrene using the built-in PerkinElmer software library (99% match). The changes to the functional groups of the inner and outer surfaces of the microplastic disks are compared in Figure 2a. The peak characteristic of the carbonyl band (~1742 cm^{-1}) was more pronounced for the aged microplastics which suggests some degree of oxidation. Indeed, the carbonyl index of the surface of the disks significantly increased after aging from 0.024 ± 0.012 to 0.068 ± 0.042, $p<0.05$ for the inner surface and from 0.0031 ± 0.0051 to 0.026 ± 0.011, $p<0.05$ for the outer surface. XPS analysis was used to complement the FTIR measurements and three different depths (depth 0 corresponding to the surface 0 nm, depth 1 corresponding to ~0.63 nm, and depth 2 corresponding to ~1.26 nm) were scanned on each side of both unaged and aged microplastics. Figure 2b-e and S6 show the O1s and C1s spectra. In the C1s spectra (Figure 2b, c), we observed an additional peak due to oxidation at the surface (depth 0) at ~289 eV which corresponds to C=O. This change is consistent on both inner and outer sides (Figure S5c, d). We observe that the oxygen content at the surface (depth 0) increased after aging (Figure 2d). The oxygen content is consistently higher for the aged microplastic, even at greater etching depth into the material (Figure 2e). Nonetheless, the extent of oxidation is greatest at the surface of the aged microplastic, and these observations are consistent on both the inner and outer surfaces of the disks (dotted and solid lines respectively, Figure 2d, e). These FTIR and XPS results confirm changes in the oxidation state and increase in hydrophilicity of the microplastics after UV treatment which is consistent with the decrease in water contact angles (discussed above).

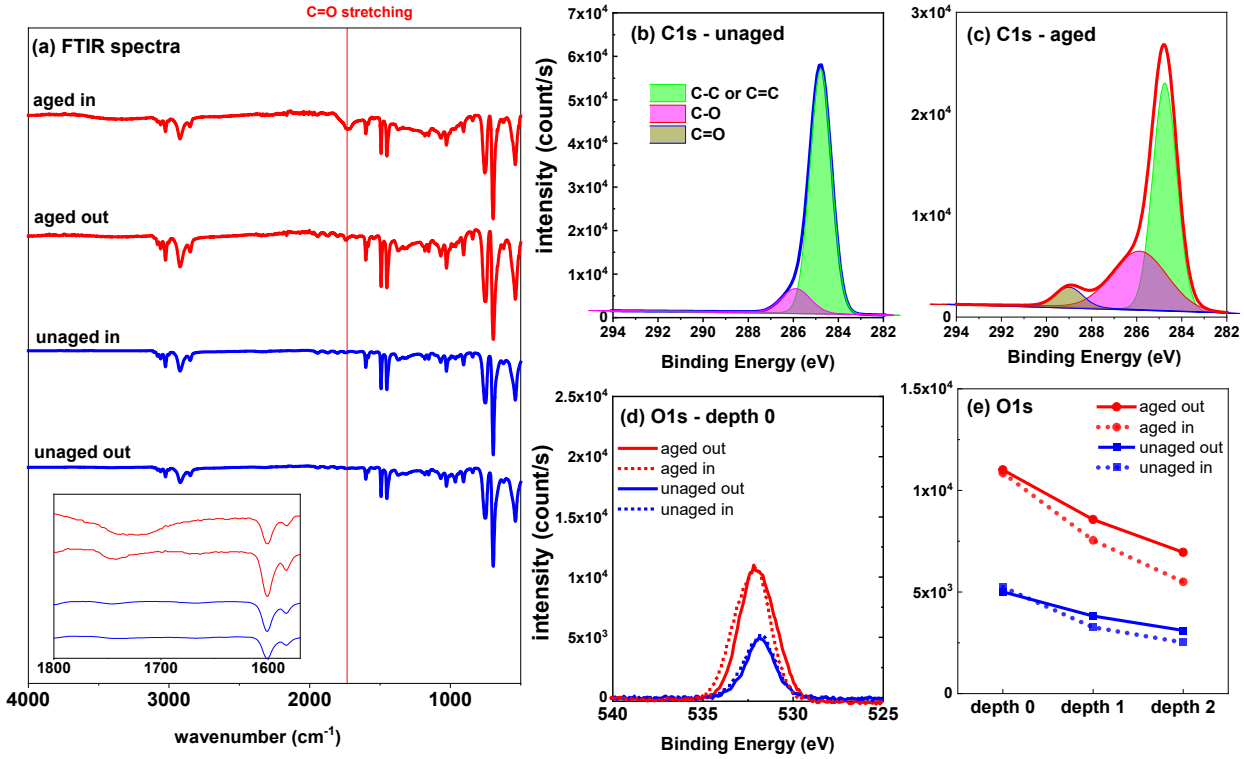

Figure 2. Surface composition characterization of microplastics. (a) representative FTIR spectra of unaged versus aged microplastics. Inset: zoom-in of FTIR spectra, (b) representative deconvoluted XPS spectra of C1s for unaged disk at depth 0, (c) representative deconvoluted XPS spectra of C1s for aged disk at depth 0, (d) XPS analysis of O1s at depth 0, (e) difference in oxygen content at depths 0, 1 and 2 for inner and outer surfaces. XPS etching done at 400 eV at 0.21 nm/s; depth 0 = outermost surface = 0 s of etching, depth 1 = 3 s and depth 2 = 6 s.

Changes in the mechanical properties of the plastic due to weathering were investigated using tensile strength tests. The experimentally measured stress versus strain curve is presented in Figure S6 while the calculated ultimate elongation and Young's modulus are reported in Table 1. Calculated Young's modulus did not change significantly after weathering, while the ultimate elongation decreased by 69% (Table 1). The reduced ultimate elongation of the aged plastics is an indication of increased brittleness, which can be associated with an increase in crystallinity (Jabarin and Lofgren, 1994). Indeed, our aged plastic samples were fragile and easy to break. Other studies also report a decrease in ultimate elongation of plastics after UV weathering (Jabarin and Lofgren, 1994; Kalogerakis et al., 2017). To summarize, we show that weathering affected the surface chemistry, tensile strength, morphology, crystallinity, surface area and density of the plastics. While the inner and outer sides of the disks were exposed to the same weathering

conditions, the two sides were not affected the same way. We also noted that the topography of the glossy outer surface of the microplastics seems to be more resistant to UV-weathering.

3.2 UV weathering increases the settling rate of polystyrene microplastics

Figure 3a shows the settling rate of the unaged versus aged microplastics. Clearly, we see an increase in the settling rate of the disks after weathering, from 0.87 ± 0.08 cm/s to 1.33 ± 0.22 cm/s (~53% increase) at 21 °C, and from 0.77 ± 0.11 cm/s to 1.19 ± 0.11 cm/s (~54% increase) at 1 °C. The mobility of particles in cold temperatures is expected to be slower compared to room temperature due to changes in fluid viscosity. Interestingly, while the percentage increase in settling velocity after weathering is similar at both temperatures, the impact of weathering is more important than that of the fluid temperature (Figure 3a). The measured increase (3%) in plastic density after weathering likely contributes to the observed increased settling rate of the disks. In addition to this change, the surface roughness and hydrophobicity of a particle could affect its drag, and hence, sinking velocity. Our surface roughness measurements showed that the microplastics became slightly rougher after weathering which would favor a reduction in settling velocity rather than an increase i.e., higher fluid-solid interactions at the plastic-water interface generate shearing and an additional drag effect. However, the contact angle measurements imply that the microplastics became more hydrophilic with aging which could play a role in decreasing the drag of the microplastics. While there are limited studies investigating the effect of UV weathering on the sinking velocity of microplastic disks, we can obtain some insights from biofouling studies. The increased settling velocity of biofouled microplastic films/sheets versus unaged microplastics has been ascribed to increased density as a result of biofilm formation on the plastic surface (Karkanorachaki et al., 2021; Miao et al., 2021). A different study shows that microplastic films from municipal plastic waste had settling velocities ranging from 0.45 – 10.47 cm/s (Van Melkebeke et al., 2020) which is in the range of our reported values. Others also reported biofouled microplastics having increased settling velocity compared to unaged ones as a result of increased density when using spherical microplastics (Kaiser et al., 2017) or irregularly shaped fragments (Semcesen and Wells, 2021).

To simulate the effect of weathering on the vertical transport of the microplastics, we need to consider that weathering affects the density and other material properties such as hydrophilicity, crystallinity, thickness or diameter which are expected to affect the drag coefficient (C_D) of the

aged disks. Hence, a correction factor (C_f) is applied to C_D for the aged microplastics. As described in section 2.7, equations 1 and 2 were used to simulate the settling velocity of different microplastic disks and spheres with similar equivalent diameters at different water temperatures. We chose microplastic spheres for comparison because spheres are often studied in the literature and their settling behavior is well predicted using validated models. For the smaller-sized disk/sphere (≤220 μm), the particles were assumed to be in the laminar regime (where Re <1). Also, a lake depth of 80 m was assumed which is representative of lake depths in Quebec, Canada (Lakelubbers, 2021), and the transport simulations are shown in Figure 3b-f. For the large microplastic disks (4.5 mm), the particles will settle out of the water column in approximately 3 and 2 hours for unaged and aged microplastics, respectively, at 21 °C. For the smaller disks (220 μm), we show that they cover the same depth in 18 and 8 days for unaged and aged microplastics, respectively. We also show in all cases (Figure 3b-f) that the unaged microplastics will travel slower at both 1 and 21 °C compared to aged microplastics at 1 °C. When the 220 μm disk is compared to spherical plastics of similar equivalent diameter (100 μm), our transport simulation revealed that microplastic disks will remain in the water column for a longer period before sinking. This is not surprising as a particle of the same diameter but that departs from a spherical shape will experience higher drag.

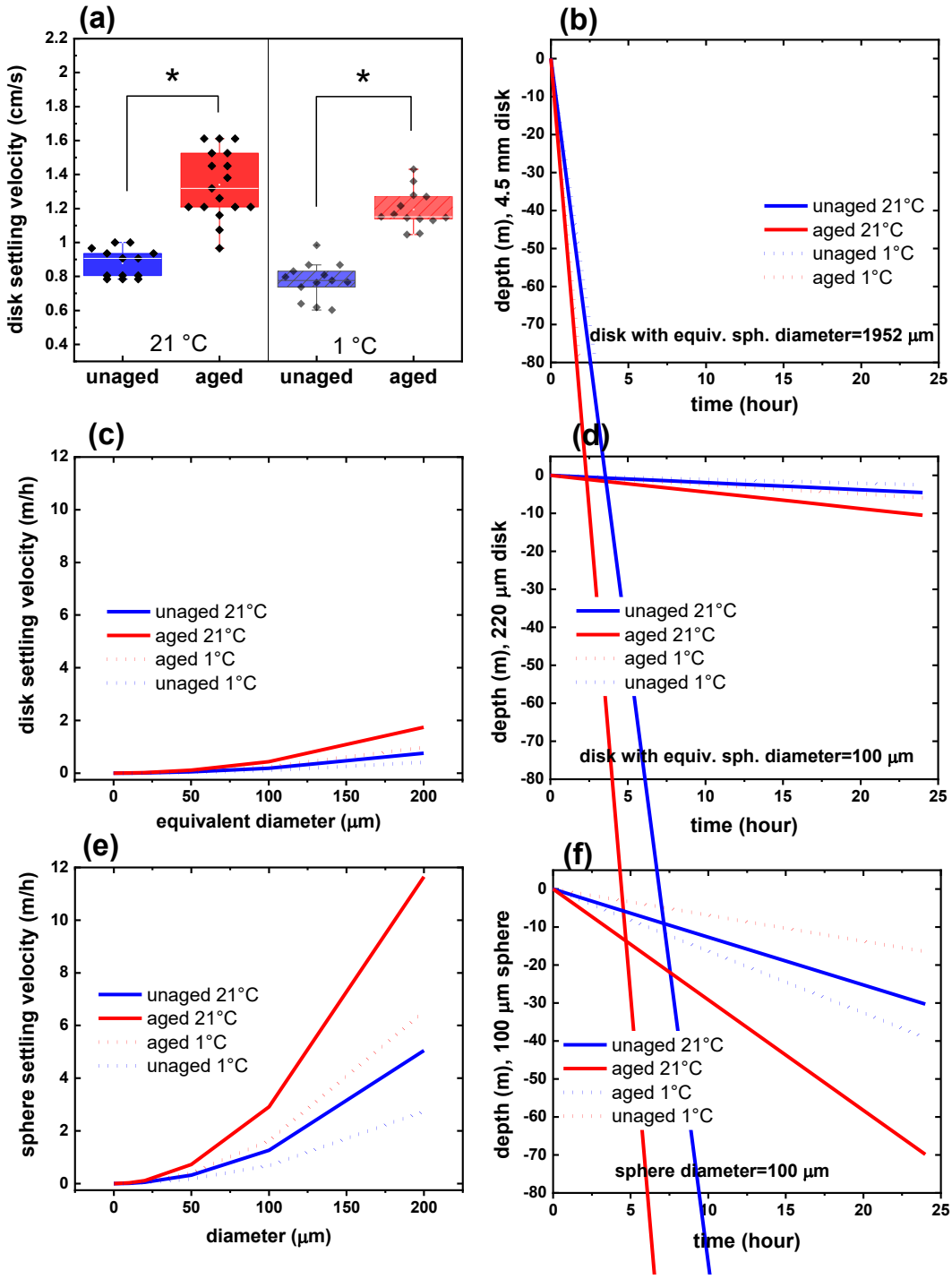

Figure 3. (a) experimental settling velocity of microplastic disks in 10 mM NaCl (d_e = 1952 µm), and (b) simulated transport distance of microplastic disks in a freshwater system (d_e = 1952 µm). (c, e) calculated settling velocity of polystyrene disk and spheres ≤200 µm, (d, f) simulated transport depth of 100 µm polystyrene disk and sphere.

3.3 Effect of weathering on adsorption capacity of triclosan on microplastics

The effect of weathering on the affinity of triclosan to the microplastics was investigated in batch sorption experiments. The adsorption kinetics of triclosan on microplastics at two concentrations (low, C_0 = 20 µg/L and high, C_0 = 100 µg /L) are shown in Figure 4a, b, while a summary of the parameters obtained from the kinetic models is presented in Table 2. Sorption equilibrium was reached for both concentrations at ~20 days. This time is higher than equilibrium times typically reported in laboratory studies investigating sorption of contaminants to primary polystyrene microplastics which range from 16 h to 17 days (Guo and Wang, 2019; Santos et al., 2021). We observed higher adsorption capacity of the unaged microplastics compared to the aged ones, only at C_0 =100 µg/L ($p < 0.05$). Both sets of kinetic experimental data fitted the pseudo-second-order model better than the first-order model, which suggests a chemisorption mechanism. The adsorption of several contaminants to microplastics has been shown to follow pseudo-second-order kinetics (Santos et al., 2021). After aging, the triclosan load (q_e) on the microplastics did not change significantly when C_0 = 20 µg/L (12.7 ± 0.4 to 13.2 ± 0.5 µg/g) but decreased at C_0 = 100 µg/L (51.4 ± 2 to 44 ± 3 µg/g, $p<0.05$). The average adsorption rate, k_2, also slightly decreased for the aged microplastics suggesting less available adsorption sites. The sorption of hydrophobic contaminants on virgin polystyrene microplastics is often attributed to several mechanisms depending on the water chemistry, contaminant, and polymer nature (Alimi et al., 2018). In our study, we hypothesize that triclosan will interact favorably with the polystyrene via hydrophobic and π-π interactions (due to the presence of benzene rings in triclosan and polystyrene). Electrostatic interaction is unlikely since triclosan is neutral at the working pH of 6. Due to the reduced hydrophobicity observed, this might explain the lower adsorption capacity of the aged microplastics. Indeed, in agreement with our study, reduced sorption was reported after aging of polystyrene microplastics for atorvastatin (Liu et al., 2020), with bisphenol A (Liu et al., 2021), and four fuel aromatics and ethers (Müller et al., 2018). In marked contrast to our work, some studies found aged polystyrene microplastics to exhibit higher sorption capacity than unaged particles for hydrophobic contaminants. For example, Xiong et al. reported that UV-aged polystyrene nanoplastics have a higher sorption capacity than unaged particles for bisphenol A (Xiong et al., 2020). Higher sorption capacities were also reported for a range of contaminants (with log K_{ow} ranging from 0.5 to 5) to thermally-aged microplastics compared to unaged ones (Ding et al., 2020). Even though the hydrophobicity of the plastic surface decreased after aging,

414 the increased sorption of aged microplastics was attributed to the higher specific surface area (Ding
415 et al., 2020). While we did observe higher surface roughness and surface area of the aged
416 microplastic disks, this did not translate to higher sorption capacities of triclosan. Interestingly, the
417 sorption capacity of the secondary polystyrene microplastics (both aged and unaged) in this study
418 is higher than some studies (Fang et al., 2019; Hai et al., 2020; Liu et al., 2021) using primary
419 polystyrene microplastics (Figure 4d). The different sorption capacities of secondary microplastics
420 in our work compared to others (Figure 4d) may be attributed to the plastic composition or type
421 used. Some manufactured plastics are known to have heterogeneous presence of fillers or additives
422 (Deanin, 1975) (which may contribute to their contaminant uptake). While we did not characterize
423 the presence of additives in our secondary microplastics, the presence of fillers is likely. Indeed,
424 microplastics with fillers have been shown to exhibit higher contaminant uptake than those without
425 fillers (Ateia et al., 2020; Zhou et al., 2022). In addition, while the studies under comparison
426 (Figure 4d) have used contaminants with comparable log K_{ow}, other unique characteristics of these
427 contaminants may provide additional mechanisms of interaction which are not observed for
428 triclosan used in this study.

429

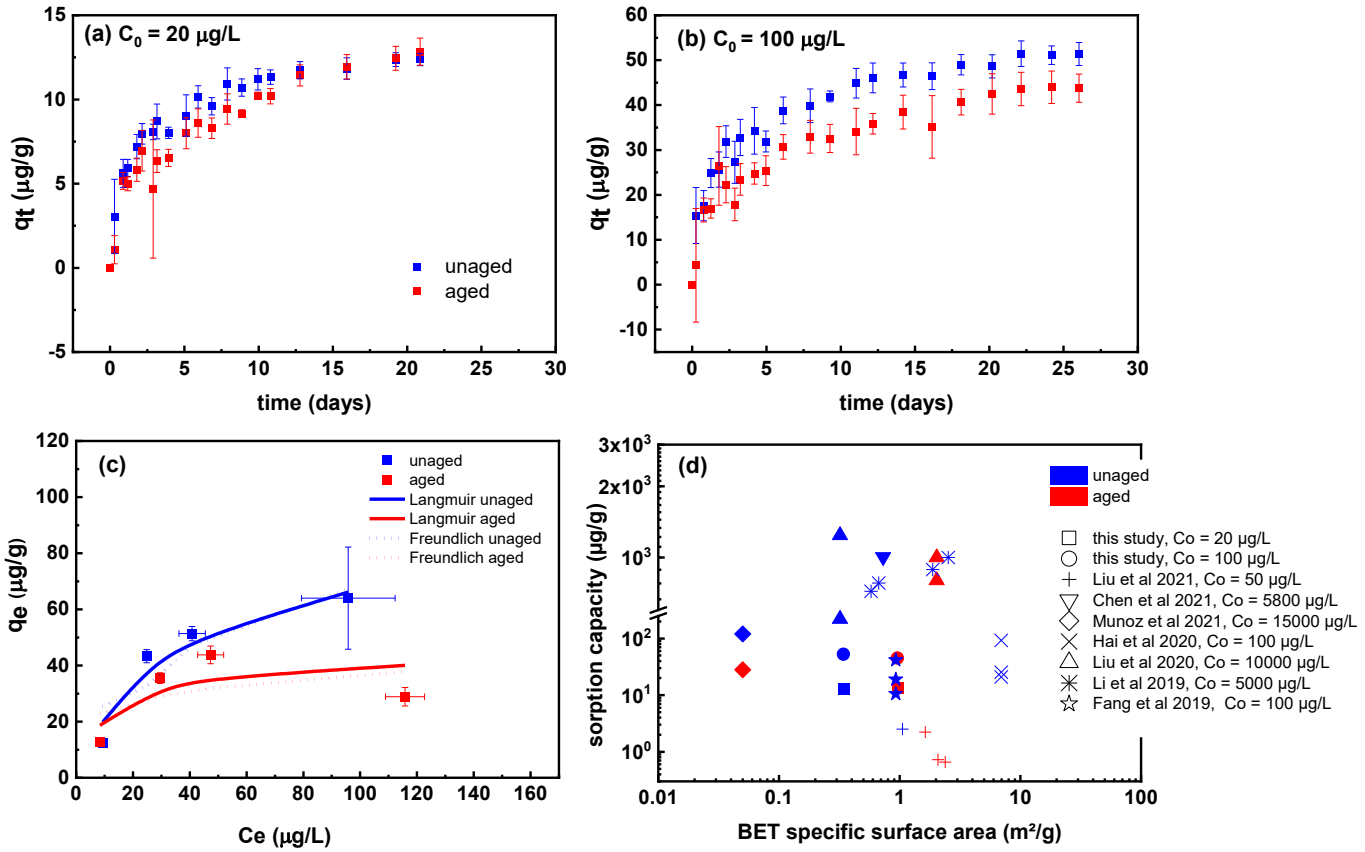

Figure 4: Effect of weathering on the (a) contaminant adsorption kinetics at 20 µg/L triclosan; (b) at 100 µg/L triclosan, (c) adsorption isotherm at pH 6, (d) comparison of hydrophobic contaminant (log K_{ow} 3.09 – 4.76) equilibrium adsorption capacity between different polystyrene microplastics in literature. Error bars denote standard deviations between triplicate runs.

From the isotherm in Figure 4c, we observe that the unaged microplastics have more affinity for triclosan at high concentration compared to the aged microplastic (that is, at C_0 = 50, 100 and 150 µg/L, $p<0.05$). Both curves follow a non-linear isotherm. Glassy polymers such as polystyrene tend to exhibit both linear and non-linear isotherms while rubbery ones such as polyethylene have linear isotherms (Hüffer and Hofmann, 2016). We can also infer from the non-linearity of the isotherm that adsorption rather than absorption is dominant which is in general agreement with previous observations (Hüffer and Hofmann, 2016). Generally, contaminants have more affinity for the amorphous region of a polymer than the crystalline region. Polystyrene is amorphous and at room temperature, it exists in a glassy state. After aging, the crystallinity increased, making the amorphous region less accessible which may contribute to the reduced sorption capacity of the

aged microplastics. By fitting the experimental data to the three isotherm models, we show that the data for unaged and aged particles fits the Langmuir model better (R^2 = 0.94 and 0.95, respectively, Table S3). This suggests a monolayer coverage of triclosan on the microplastic surface.

Table 2. Kinetic model fitting parameters for triclosan adsorption and desorption on microplastics

model	parameter	unaged	aged
Adsorption, C_0 = 20 μg/L	$q_{e,\,exp}$ (μg/g)	12 ± 0.36	13 ± 0.81
Pseudo-first order	k_1 (day^{-1})	0.53 ± 0.11	0.25 ± 0.044
	q_e (μg/g)	11 ± 0.38	12 ± 1.07
	R^2	0.89 ± 0.04	0.86 ± 0.057
Pseudo-second order	k_2 ($g(\mu g.day)^{-1}$)	0.058 ± 0.017	0.029 ± 0.0065
	q_e (μg/g)	13 ± 0.39	13 ± 0.51
	R^2	0.95 ± 0.023	0.93 ± 0.0098
Adsorption, C_0 = 100 μg/L	$q_{e,\,exp}$ (μg/g)	51 ± 2.6	44 ± 3.1
Pseudo-first order	k_1 (day^{-1})	0.39 ± 0.105	0.31 ± 0.015
	q_e (μg/g)	47 ± 2.3	39 ± 4.7
	R^2	0.87 ± 0.05	0.81 ± 0.095
Pseudo-second order	k_2 ($g(\mu g.day)^{-1}$)	0.011 ± 0.004	0.0084 ± 0.0010
	q_e (μg/g)	53 ± 2.5	45 ± 3.5
	R^2	0.93 ± 0.030	0.87 ± 0.069
Desorption, C_0 = 100 μg/L	$q_{e,\,exp}$ (μg/g)	42 ± 2.8	38 ± 3.3
Pseudo-first order	k_1 (day^{-1})	0.49 ± 0.069	0.60 ± 0.14
	q_e (μg/g)	42 ± 3.7	38 ± 3.3
	R^2	0.71 ± 0.041	0.97 ± 0.008
Pseudo-second order	k_2 ($g(\mu g.day)^{-1}$)	0.081 ± 0.0081	0.13 ± 0.04
	q_e (μg/g)	43 ± 2.70	38 ± 3.3
	R^2	0.98 ± 0.0046	0.98 ± 0.0079

$q_{e,\,exp}$ = experimental adsorption capacity at equilibrium

3.4 Effect of weathering on desorption of triclosan from microplastics and potential for facilitated transport

To understand the potential for release of contaminants in freshwater systems, the desorption kinetics of triclosan from the microplastic disks was monitored in 10 mM NaCl solutions at C_0 = 100 µg/L. Desorption kinetics as well as adsorption and desorption isotherms are shown in Figure 5a, b and c, respectively. First, we observe that the aged and unaged microplastics reached desorption equilibrium after 5 days (Figure 5a), which is fast compared to the adsorption time of ~20 days. The desorption kinetic data was well fitted to the pseudo-second-order model (Table 1). Interestingly, at equilibrium, more triclosan desorbed from the unaged microplastics compared to the aged ones (C_e = 7.9±0.10 vs 5.1±0.33 µg/L respectively, $p<0.05$) even though there was no significant difference in their desorption rates (k_2 = 0.081 ± 0.008 vs 0.13 ± 0.04 g/µg.day, respectively, $p> 0.05$). The higher C_e observed for unaged versus aged disks is consistent across a range of starting concentrations (Figure S7). Perhaps the aged microplastics did not release more triclosan because of their initial low adsorption capacity, q_e compared to the unaged microplastics. In the isotherm plot, adsorption and desorption hysteresis is observed for both unaged (Figure 5b) and aged microplastics (Figure 5c) implying that the adsorption of triclosan by the microplastics is not fully reversible for the tested conditions. This is consistent with the calculated hysteresis indices (HI, Figure 5b, c). When HI is ≤ 0, desorption hysteresis is not obvious while the greater the HI value, the higher the degree of hysteresis (Liu et al., 2018). The calculated hysteresis indices are generally > 0 except for one value for aged microplastics (Figure 5c) which is slightly negative/neutral. The glassy domains in polymeric structures (e.g., polystyrene and geocolloids) have been reported to be favorable for adsorption but energetically unfavorable for desorption of non-polar hydrophobic molecules (Liu et al., 2018; Luthy et al., 1997). Liu et al. showed how pyrene was irreversibly adsorbed to polystyrene compared to a rubbery polymer, polyethylene (Liu et al., 2018). This may explain the hysteresis observed during desorption. We also observe from the desorption isotherm that generally, the unaged microplastics retain more triclosan than the aged ones (Figure 5b, c, Table S3).

Triclosan desorption kinetics of unaged and aged disks (Figure 5a) were combined with the measured settling rates (Figure 3a) to quantify the amount of triclosan released as function of time and depth in natural waters (simulated for a lake of 80 m depth where the horizontal flow was

assumed to be negligible). Because of their higher settling rate, aged disks would release triclosan deeper in the water column compared to unaged disks. To account for the microplastic shape, simulations were also performed on a 220 µm disk (having equivalent spherical diameter of 100 µm) and spherical microplastic (100 µm). Assuming that the desorption kinetics presented in Figure 5a are conserved for a microplastic with an equivalent spherical diameter of 100 µm it is more likely that aged disks and spherical microplastics would release triclosan at the bottom of a lake (i.e., in sediments), while the unaged and non-spherical microplastics are more likely to release triclosan in the water column (Figure S8).

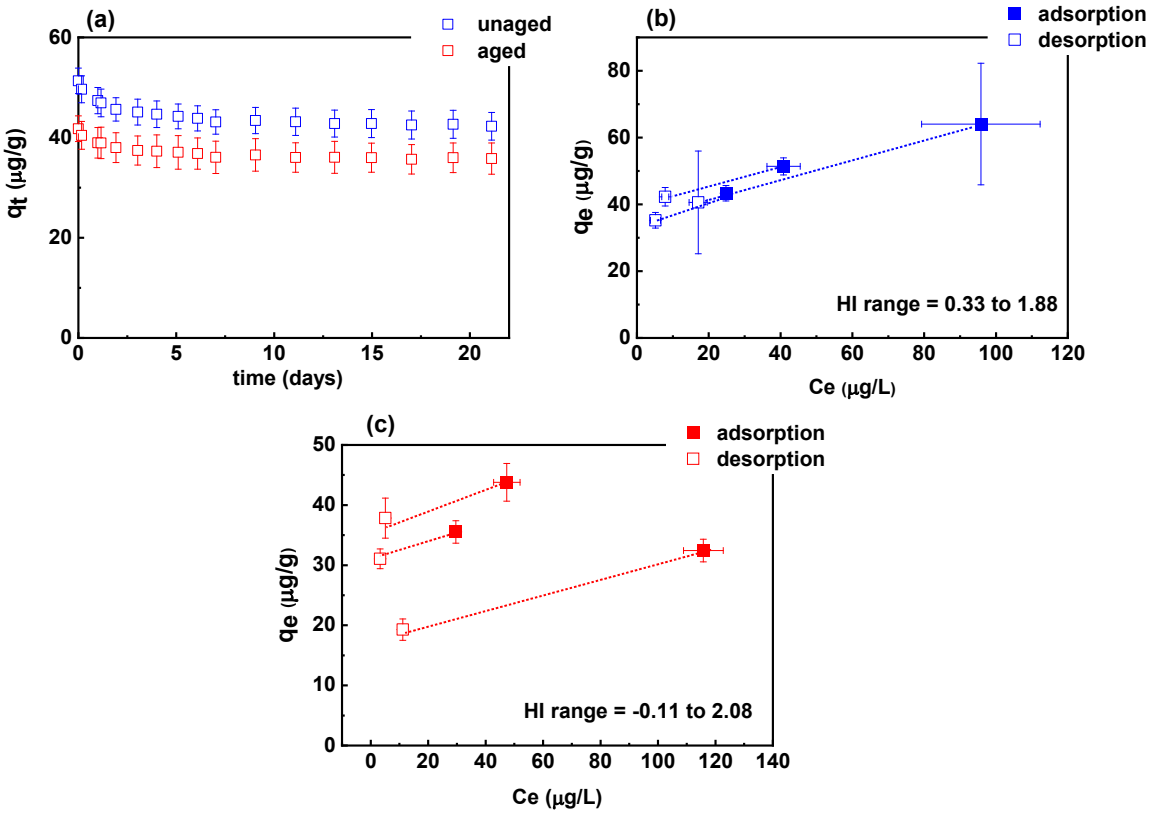

Figure 5: Desorption data for triclosan in 10 mM NaCl. (a) desorption kinetics at C_0 = 100 µg/L, (b) desorption isotherm of unaged microplastics, (c) desorption isotherm of aged microplastics. Dotted line drawn to connect each adsorption data with its desorption data. Error bars denote standard deviations of 3 experimental runs. HI = hysteresis index.

4. Conclusions

The effect of weathering on the transport and contaminant facilitated transport of microplastics in surface waters is largely underexplored. While some efforts have been made to understand the transport potential of microplastics in the aquatic environment, the use of unaged plastics limits our understanding of the risks associated with environmentally relevant microplastics. We report novel findings on the effect of UV-weathering on the settling velocity of secondary polystyrene microplastics and their interaction with an organic contaminant. We show that weathering will transform some physicochemical and mechanical properties of microplastic disks obtained from a single-use cup which includes the surface roughness, density, surface chemistry, wettability, crystallinity, and tensile strength. These transformations affected the fate, transport, and interactions of the microplastics with triclosan in a model aquatic environment.

Specifically, our experimental data reveals that UV weathering led to increased transport and that this impact of weathering outweighs the effect of water temperature. Considering a lake in Quebec as a case study and based on the settling velocities measured, simulations show that weathering will reduce the residence time of a microplastic disk from 3 to 2 hours and 18 to 8 days (for 4.5 mm and 0.220 mm sizes, respectively). Two recent studies reported an increased settling rate of aged (biofouled) microplastic films/sheets in natural water samples (Karkanorachaki et al., 2021; Miao et al., 2021). While the weathering design in our study (simple water matrix, 10 mM NaCl) was not aimed at producing biofouled microplastics or grow biofilms on microplastics, we show that other transformations (which may include changes in density and crystallinity of the microplastics) as a result of UV degradation could increase the sinking rates and transport of microplastics. The settling velocity and transport reported in our work for aged microplastics is expected to be even higher when natural colloids or biofilms are attached to the aged microplastics.

Our results also show that aged polystyrene microplastics can have a lower affinity for a model hydrophobic contaminant, triclosan and the unaged polystyrene microplastic partially desorbs more contaminant compared to the aged material. These results suggest that microplastics from bulk plastic debris may act as vectors for hydrophobic contaminants when in a “cleaner” water body or potentially to an organism when ingested. Despite the low working contaminant concentration (ppb range) and low specific surface area of the microplastic disks used in our study, we still observe higher adsorption of a hydrophobic contaminant than some primary microplastic

types with higher specific surface areas in literature (Fang et al., 2019; Hai et al., 2020; Liu et al., 2021). Indeed, there is a need for more studies using microplastics of environmental relevance rather than unaged primary polymers.

The observed lower contaminant sorption and desorption potential as well as the faster settling rates of aged polystyrene microplastics compared to unaged ones, suggests that the aged plastics may barely facilitate the mobility of hydrophobic contaminants (such as triclosan) in surface waters.

Acknowledgments

The authors acknowledge the support of the Canada Research Chairs program, the Natural Sciences and Engineering Research Council of Canada, the Canada Banting Fellowship program, the Killam Research Fellowship program, the Canada Foundation for Innovation/John R. Evans Leaders Fund grant (Project #35318 of S. Bayen), the Petroleum Technology Development Fund of Nigeria, the Fonds Quebecois de la recherche sur la nature et les technologies (FQRNT), and the Eugenie Ulmer Lamothe Fund at McGill for awards to OSA. This project was supported partially by a financial contribution from Fisheries and Oceans Canada. The authors would like to acknowledge M. Sander at ETH Zurich for his helpful insights and comments during the design of the adsorption experiments. We thank R. Leask for access to the tensile testing instrument. We also thank L. Rowenczyk and R. Salles Kurusu for helpful discussions about plastic characterization.

CRediT Authorship Contribution Statement

Olubukola S. Alimi: Conceptualization, Writing – original draft, Methodology, Data Curation, Formal Analysis, Visualization, Investigation. **Dominique Claveau-Mallet:** Conceptualization, Methodology, Writing – review & editing**,** Visualization, Investigation. **Mathieu Lapointe:** Writing – review & editing**,** Formal Analysis**,** Visualization **Thinh Biu:** Writing – review & editing, Investigation, Methodology. **Lan Liu:** Writing – review & editing, Investigation. **Laura M. Hernandez:** Writing – review & editing, Investigation**. Stéphane Bayen:** Conceptualization, Supervision, Writing – review & editing. **Nathalie Tufenkji:** Conceptualization, Supervision, Writing – review & editing.

References

Alimi, O.S., Claveau-Mallet, D., Kurusu, R.S., Lapointe, M., Bayen, S. and Tufenkji, N. 2022. Weathering pathways and protocols for environmentally relevant microplastics and nanoplastics: What are we missing? *J. Hazard. Mater.* 423, 126955.

Alimi, O.S., Farner Budarz, J., Hernandez, L.M. and Tufenkji, N. 2018. Microplastics and nanoplastics in aquatic environments: Aggregation, deposition, and enhanced contaminant transport. *Environ. Sci. Technol.* 52(4), 1704-1724.

Alimi, O.S., Farner, J.M. and Tufenkji, N. 2020. Exposure of nanoplastics to freeze-thaw leads to aggregation and reduced transport in model groundwater environments. *Water Res.*, 116533.

Almond, J., Sugumaar, P., Wenzel, M.N., Hill, G. and Wallis, C. 2020. Determination of the carbonyl index of polyethylene and polypropylene using specified area under band methodology with ATR-FTIR spectroscopy. *e-Polymers* 20(1), 369-381.

Andrady, A.L. 2011. Microplastics in the marine environment. *Mar. Pollut. Bull.* 62(8), 1596-1605.

Andrady, A.L., Hamid, S.H., Hu, X. and Torikai, A. 1998. Effects of increased solar ultraviolet radiation on materials. *J. Photochem. Photobiol. B: Biol.* 46(1), 96-103.

Ateia, M., Zheng, T., Calace, S., Tharayil, N., Pilla, S. and Karanfil, T. 2020. Sorption behavior of real microplastics (MPs): Insights for organic micropollutants adsorption on a large set of well-characterized MPs. *Sci. Total Environ.* 720, 137634.

Barrett, H., Sun, J., Gong, Y., Yang, P., Hao, C., Verreault, J., Zhang, Y. and Peng, H. 2022. Triclosan is the Predominant Antibacterial Compound in Ontario Sewage Sludge. *Environ. Sci. Technol.*

Borrelle, S.B., Ringma, J., Law, K.L., Monnahan, C.C., Lebreton, L., McGivern, A., Murphy, E., Jambeck, J., Leonard, G.H. and Hilleary, M.A. 2020. Predicted growth in plastic waste exceeds efforts to mitigate plastic pollution. *Sci* 369(6510), 1515-1518.

Boucher, J. and Friot, D. (2017) Primary microplastics in the oceans: a global evaluation of sources, IUCN Gland, Switzerland.

Deanin, R.D. 1975. Additives in plastics. *Environ. Health Perspect.* 11, 35-39.

Ding, L., Mao, R., Ma, S., Guo, X. and Zhu, L. 2020. High temperature depended on the ageing mechanism of microplastics under different environmental conditions and its effect on the distribution of organic pollutants. *Water Res.* 174, 115634.

Fang, S., Yu, W.S., Li, C.L., Liu, Y.D., Qiu, J. and Kong, F.Y. 2019. Adsorption behavior of three triazole fungicides on polystyrene microplastics. *Sci. Total Environ.* 691, 1119.

Geyer, R. (2020) Plastic Waste and Recycling. Letcher, T.M. (ed), pp. 13-32, Academic Press.

Guo, X. and Wang, J. 2019. The chemical behaviors of microplastics in marine environment: A review. *Mar. Pollut. Bull.* 142, 1-14.

Hai, N., Liu, X., Li, Y., Kong, F., Zhang, Y. and Fang, S. 2020. Effects of microplastics on the adsorption and bioavailability of three strobilurin fungicides. *ACS Omega* 5(47), 30679-30686.

Hüffer, T. and Hofmann, T. 2016. Sorption of non-polar organic compounds by micro-sized plastic particles in aqueous solution. *Environ. Pollut.* 214(17), 194-201.

ISO-1183-1 2019 Plastics—Methods for Determining the Density of Non Cellular Plastics—Part 1: IMMERSION Method, Liquid Pycnometer Method and Titration Method, ISO Geneva, Switzerland.

Jabarin, S.A. and Lofgren, E.A. 1994. Photooxidative effects on properties and structure of high-density polyethylene. *J. Appl. Polym. Sci.* 53(4), 411-423.

Jahnke, A., Arp, H.P.H., Escher, B.I., Gewert, B., Gorokhova, E., Kühnel, D., Ogonowski, M., Potthoff, A., Rummel, C., Schmitt-Jansen, M., Toorman, E. and MacLeod, M. 2017. Reducing uncertainty and confronting ignorance about the possible impacts of weathering plastic in the marine environment. *Environ. Sci. Technol. Letters* 4(3), 85-90.

Kaiser, D., Kowalski, N. and Waniek, J.J. 2017. Effects of biofouling on the sinking behavior of microplastics. *Environ. Res. Lett.* 12(12), 124003.

Kalogerakis, N., Karkanorachaki, K., Kalogerakis, G.C., Triantafyllidi, E.I., Gotsis, A.D., Partsinevelos, P. and Fava, F. 2017. Microplastics generation: Onset of fragmentation of polyethylene films in marine environment mesocosms. *Front. Mar. Sci.* 4(84).

Karkanorachaki, K., Syranidou, E. and Kalogerakis, N. 2021. Sinking characteristics of microplastics in the marine environment. *Sci. Total Environ.* 793, 148526.

Katz, B.G., DeHan, R.S., Hirten, J.J. and Catches, J.S. 1997. Interactions Between Ground Water And Surface Water In The Suwannee River Basin, Florida 1. *JAWRA Journal of the American Water Resources Association* 33(6), 1237-1254.

Kooi, M., Nes, E.H.v., Scheffer, M. and Koelmans, A.A. 2017. Ups and Downs in the Ocean: Effects of Biofouling on Vertical Transport of Microplastics. *Environ. Sci. Technol.* 51(14), 7963-7971.

Krause, S., Molari, M., Gorb, E.V., Gorb, S.N., Kossel, E. and Haeckel, M. 2020. Persistence of plastic debris and its colonization by bacterial communities after two decades on the abyssal seafloor. *Sci. Rep.* 10(1), 9484.

Kumar, K.S., Priya, S.M., Peck, A.M. and Sajwan, K.S. 2010. Mass loadings of triclosan and triclocarbon from four wastewater treatment plants to three rivers and landfill in Savannah, Georgia, USA. *Arch. Environ. Contam. Toxicol.* 58, 275-285.

Lakelubbers 2021 Quebec deep lakes in Quebec, pp. www.lakelubbers.com/quebec-deep-lakes-in-quebec.

Lau, W.W.Y., Shiran, Y., Bailey, R.M., Cook, E., Stuchtey, M.R., Koskella, J., Velis, C.A., Godfrey, L., Boucher, J., Murphy, M.B., Thompson, R.C., Jankowska, E., Castillo Castillo, A., Pilditch, T.D., Dixon, B., Koerselman, L., Kosior, E., Favoino, E., Gutberlet, J., Baulch, S., Atreya, M.E., Fischer, D., He, K.K., Petit, M.M., Sumaila, U.R., Neil, E., Bernhofen, M.V., Lawrence, K. and Palardy, J.E. 2020. Evaluating scenarios toward zero plastic pollution. *Sci* 369(6510), 1455-1461.

Lindström, A., Buerge, I.J., Poiger, T., Bergqvist, P.-A., Müller, M.D. and Buser, H.-R. 2002. Occurrence and Environmental Behavior of the Bactericide Triclosan and Its Methyl Derivative in Surface Waters and in Wastewater. *Environ. Sci. Technol.* 36(11), 2322-2329.

Liu, J., Ma, Y., Zhu, D., Xia, T., Qi, Y., Yao, Y., Guo, X., Ji, R. and Chen, W. 2018. Polystyrene nanoplastics-enhanced contaminant transport: Role of irreversible adsorption in glassy polymeric domain. *Environ. Sci. Technol.* 52(5), 2677-2685.

Liu, P., Lu, K., Li, J., Wu, X., Qian, L., Wang, M. and Gao, S. 2020. Effect of aging on adsorption behavior of polystyrene microplastics for pharmaceuticals: Adsorption mechanism and role of aging intermediates. *J. Hazard. Mater.* 384, 121193.

Liu, X., Sun, P., Qu, G., Jing, J., Zhang, T., Shi, H. and Zhao, Y. 2021. Insight into the characteristics and sorption behaviors of aged polystyrene microplastics through three type of accelerated oxidation processes. *J. Hazard. Mater.* 407, 124836.

Lobelle, D., Kooi, M., Koelmans, A.A., Laufkötter, C., Jongedijk, C.E., Kehl, C. and van Sebille, E. 2021. Global modeled sinking characteristics of biofouled microplastic. *J. Geophys. Res. Oceans* 126(4), e2020JC017098.

Luthy, R.G., Aiken, G.R., Brusseau, M.L., Cunningham, S.D., Gschwend, P.M., Pignatello, J.J., Reinhard, M., Traina, S.J., Weber, W.J. and Westall, J.C. 1997. Sequestration of hydrophobic organic contaminants by geosorbents. *Environ. Sci. Technol.* 31(12), 3341-3347.

Miao, L., Gao, Y., Adyel, T.M., Huo, Z., Liu, Z., Wu, J. and Hou, J. 2021. Effects of biofilm colonization on the sinking of microplastics in three freshwater environments. *J. Hazard. Mater.* 413, 125370.

Müller, A., Becker, R., Dorgerloh, U., Simon, F.G. and Braun, U. 2018. The effect of polymer aging on the uptake of fuel aromatics and ethers by microplastics. *Environ. Pollut.* 240, 639-646.

Nguyen, T.H., Tang, F.H.M. and Maggi, F. 2020. Sinking of microbial-associated microplastics in natural waters. *PLoS One* 15(2), e0228209.

Pullaguri, N., Umale, A. and Bhargava, A. 2023. Neurotoxic mechanisms of triclosan: The antimicrobial agent emerging as a toxicant. *J. Biochem. Mol. Toxicol.* 37(2), e23244.

Ramaswamy, B.R., Shanmugam, G., Velu, G., Rengarajan, B. and Larsson, D.J. 2011. GC–MS analysis and ecotoxicological risk assessment of triclosan, carbamazepine and parabens in Indian rivers. *J. Hazard. Mater.* 186(2-3), 1586-1593.

Rochman, C.M., Manzano, C., Hentschel, B.T., Simonich, S.L. and Hoh, E. 2013. Polystyrene plastic: a source and sink for polycyclic aromatic hydrocarbons in the marine environment. *Environ. Sci. Technol.* 47(24), 13976-13984.

Rowenczyk, L., Dazzi, A., Deniset-Besseau, A., Beltran, V., Goudounèche, D., Wong-Wah-Chung, P., Boyron, O., George, M., Fabre, P. and Roux, C. 2020. Microstructure characterization of oceanic polyethylene debris. *Environ. Sci. Technol.* 54(7), 4102-4109.

Rudin, A. and Choi, P. 2013. Mechanical properties of polymer solids and liquids. *The Elements of Polymer Science & Engineering* 3.

Santos, L.H.M.L.M., Rodríguez-Mozaz, S. and Barceló, D. 2021. Microplastics as vectors of pharmaceuticals in aquatic organisms – An overview of their environmental implications. *Case Studies in Chemical and Environmental Engineering* 3, 100079.

Saron, C., Sanchez, E.M. and Isabel Felisberti, M. 2007. Thermal and photochemical degradation of PPO/HIPS blends. *J. Appl. Polym. Sci.* 104(5), 3269-3276.

Semcesen, P.O. and Wells, M.G. 2021. Biofilm growth on buoyant microplastics leads to changes in settling rates: Implications for microplastic retention in the Great Lakes. *Mar. Pollut. Bull.* 170, 112573.

Stowe, B.S., Salvin, V., Fornes, R. and Gilbert, R. 1973. The effect of near-ultraviolet radiation on the morphology of nylon 66. *Text. Res. J.* 43(12), 704-714.

Van Melkebeke, M., Janssen, C. and De Meester, S. 2020. Characteristics and sinking behavior of typical microplastics including the potential effect of biofouling: Implications for remediation. *Environ. Sci. Technol.* 54(14), 8668-8680.

Waldschläger, K., Born, M., Cowger, W., Gray, A. and Schüttrumpf, H. 2020. Settling and rising velocities of environmentally weathered micro-and macroplastic particles. *Environ. Res.*, 110192.

Waldschläger, K. and Schüttrumpf, H. 2019. Effects of particle properties on the settling and rise velocities of microplastics in freshwater under laboratory conditions. *Environ. Sci. Technol.* 53(4), 1958-1966.

Xiong, Y., Zhao, J., Li, L., Wang, Y., Dai, X., Yu, F. and Ma, J. 2020. Interfacial interaction between micro/nanoplastics and typical PPCPs and nanoplastics removal via electrosorption from an aqueous solution. *Water Res.*, 116100.

Zhang, Y., Liang, J., Zeng, G., Tang, W., Lu, Y., Luo, Y., Xing, W., Tang, N., Ye, S. and Li, X. 2020. How climate change and eutrophication interact with microplastic pollution and sediment resuspension in shallow lakes: A review. *Sci. Total Environ.* 705, 135979.

Zhou, J., Chen, H., Guo, Y., Chen, Q., Ren, H. and Tao, Y. 2022. Changes in metal adsorption ability of microplastics upon loss of calcium carbonate filler masterbatch through natural aging. *Sci. Total Environ.* 832, 155142.